

Synthesis and characterization of PVP-functionalized superparamagnetic Fe₃O₄ nanoparticles as an MRI contrast agent

N. Arsalani^{1*}, H. Fattahi¹, M. Nazarpour²

¹Polymer Research Laboratory, Department of Organic and Biochemistry, Faculty of Chemistry, University of Tabriz, Tabriz, Iran

²Department of Radiology, Faculty of Paramedical, Tabriz University of Medical Sciences, Tabriz, Iran

Received 21 January 2010; accepted in revised form 19 March 2010

Abstract. The magnetite (Fe₃O₄) nanoparticles (MNPs) coated with poly(N-vinyl pyrrolidone) (PVP) via covalent bonds were prepared as *T*₂ contrast agent for magnetic resonance imaging (MRI). The surface of MNPs was first coated with 3-(trimethoxysilyl) propyl methacrylate (silan A) by a silanization reaction to introduce reactive vinyl groups onto the surface, then poly(N-vinyl pyrrolidone) was grafted onto the surface of modified-MNPs via surface-initiated radical polymerization. The obtained nanoparticles were characterized by FT-IR (Fourier transform infrared spectroscopy), XRD (X-ray diffraction), TEM (transmission electron microscopy), VSM (vibrating sample magnetometer), and TGA (thermogravimetric analysis). The MNPs had an average size of 14 nm and exhibited superparamagnetism and high saturation magnetization at room temperature. *T*₂-weighted MRI images of PVP-grafted MNPs showed that the magnetic resonance signal is enhanced significantly with increasing nanoparticle concentration in water. The *r*₁ and *r*₂ values per millimole Fe, and *r*₂/*r*₁ value of the PVP-grafted MNPs were calculated to be 2.6, 72.1, and 28.1(mmol/l)⁻¹·s⁻¹, respectively. These results indicate that the PVP-grafted MNPs have great potential for application in MRI as a *T*₂ contrast agent.

Keywords: *nanomaterials, superparamagnetism, iron oxide nanoparticles, MRI contrast agent*

1. Introduction

In recent years, superparamagnetic iron oxide nanoparticles have shown great potential applications in many biological fields, including targeted-drug delivery [1, 2], bioseparation [3], tissue repair [4], cancer treatment through hyperthermia [5, 6], and magnetic resonance imaging (MRI) contrast enhancement [7–9].

MRI is an appealing noninvasive approach for early cancer diagnostics and therapeutics [10]. However, in clinical diagnosis, it is often the case that the diseased and healthy tissues are similar in composition and MRI technology alone will not always differentiate the two. A contrast agent is necessary to distinguish the normal and diseased

tissue. The conventional, gadolinium compounds [11] have been used as *T*₁ contrast agents that cause positive contrast enhancement and provide a bright state in the image where the compounds are accumulated [12]. However, with the increasing use of paramagnetic gadolinium chelates for MRI, shortcomings of gadolinium chelates have been found, such as fast elimination in tissue; non-specific distribution in vivo and limited effect in improving MR imaging.

Since superparamagnetic Fe₃O₄ nanoparticles can enhance the alterations of proton relaxation in the tissue microenvironment, these are suitable as *T*₂ contrast agent in MRI [13, 14]. These *T*₂ contrast agents cause to decrease the signal intensity in the

*Corresponding author, e-mail: arsalani@tabrizu.ac.ir
© BME-PT

region that they are accumulated, and hence cause negative contrast and provide a dark state in the image where the compounds are accumulated [15]. However, the direct use of magnetic nanoparticles as in vivo MRI contrast agent results in biofouling of the particles in blood plasma and formation of aggregates that are quickly sequestered by cells of the reticular endothelial system (RES) such as macrophages [16, 17]. Furthermore, aggregated nanoparticles change their superparamagnetic response [7]. Therefore, in order to minimize biofouling and aggregation of particles and escape from the RES for longer circulation times, the nanoparticles are usually coated with a layer of hydrophilic and biocompatible polymer such as dextran [18], dendrimers [19], poly(ethylene glycol) (PEG) [20], and poly(vinyl pyrrolidone) (PVP) [21–23]. Of synthetic polymers, PVP is water-soluble, non-charged, non-toxic, and is used in various medical applications [24]. While there is a potential concern about covalent interaction between hydrophilic polymers and magnetic nanoparticles in order to increase their stability in physiological medium [25–29], PVP coating on Fe_3O_4 nanoparticles in all previous works has been achieved through noncovalent interaction.

Now, polymers grafting of magnetic nanoparticles is one of the most attractive methods of surface modification [30, 31]. In the present study, we carried out chemical synthesis and characterization of PVP-functionalized magnetite (Fe_3O_4) nanoparticles. Since the PVP was bonded to the surface of magnetite nanoparticles through covalent bonds, the prepared magnetic fluid (ferrofluid) was very stable for a long period of time. To this aim, first magnetite nanoparticles were synthesized by the chemical co-precipitation of Fe^{3+} and Fe^{2+} ions with NH_4OH . Then, the nanoparticles were modified directly by 3-(trimethoxysilyl) propyl methacrylate (silan A) to introduce reactive vinyl groups on the particles surface, and poly(N-vinyl pyrrolidone) was grafted onto modified nanoparticles by surface-initiated radical polymerization. The structure, particle size, and composition of PVP-functionalized magnetite nanoparticles were examined by FT-IR (Fourier transform infrared spectroscopy), XRD (X-ray diffraction), TEM (transmission electron microscopy), VSM (vibrating sample magnetometer), and TGA (thermogravimetric analysis). Furthermore, the PVP-functionalized MNPs were

dispersed in water to form stable magnetic fluids. T_2 -weighted MRI images of PVP-grafted magnetic nanoparticles were obtained and the results indicated that they have great potential for application in MRI as T_2 contrast agent.

2. Experimental

2.1. Materials

Ferric chloride hexahydrate ($\text{FeCl}_3 \cdot 6\text{H}_2\text{O}$, >99%), ferrous chloride tetrahydrate ($\text{FeCl}_2 \cdot 4\text{H}_2\text{O}$, >99%) and ammonium hydroxide (25 wt%) were obtained from Fluka (Switzerland). 3-(trimethoxysilyl) propyl methacrylate (silan A), dichloromethane and Azobisisobutyronitrile (AIBN) were purchased from Merck (Schuchardt, Germany). All the materials mentioned above were used without further purification. N-vinyl pyrrolidone was obtained from Merck (Schuchardt, Germany) and was distilled under reduced pressure prior to use. Ethanol (96%) was provided by Simin Tak (Qazvin, Iran). Distilled water was used throughout the work.

2.2. Synthesis of Fe_3O_4 nanoparticles

The preparation of Fe_3O_4 nanoparticles was followed by a chemical co-precipitation of Fe^{2+} and Fe^{3+} ions described previously [32]. Briefly, fifty milliliters of 1.0 mol/l Fe^{2+} and 2.0 mol/l Fe^{3+} solutions were prepared with deionized water in two beakers, and then transferred to a 250 ml three-necked flask together. When the solution was heated to 80°C , NH_4OH (25 wt%) was added dropwise under argon protection and vigorous mechanical stirring until $\text{pH} = 10\text{--}11$. As the base was added, the solution immediately turned black indicating the formation of iron oxide in the system. The solution was heated at 80°C for 1 h, and then the precipitated powders were collected by magnetic separation. The obtained magnetic nanoparticles were washed immediately with deionized water for five times and then with dichloromethane for three times. The final product was dried into powder at 40°C under vacuum.

2.3. Preparation of silan A-modified Fe_3O_4 nanoparticles

In order to introduce vinyl group onto the magnetic nanoparticles, we used 3-(trimethoxysilyl) propyl

methacrylate (silan A) as a coupling agent. Silan A-modified magnetic nanoparticles were achieved by the silanization reaction between Silan A and the hydroxyl groups on the surface of magnetite. Namely, 3.7 g of Fe_3O_4 nanoparticles were dispersed in 40 ml toluene by sonication for about 1 h, and then 19.5 mmol (4.66 ml) of Silan A was added under argon atmosphere using a syringe. The reaction mixture was kept at room temperature for 5 h with vigorous mechanical stirring. Afterwards, the Silan A-immobilized Fe_3O_4 nanoparticles were obtained by magnetic separation and washed with ethanol (2×30 ml) and dichloromethane (2×30 ml) in turn. They were then dried in a vacuum oven at 40°C overnight.

2.4. Synthesis of PVP-grafted Fe_3O_4 nanoparticles

The graft polymerization was performed using surface-initiated radical polymerization, according to a modified procedure [31]. In a typical protocol, 0.5 g of silan A-modified Fe_3O_4 nanoparticles, 0.069 g of AIBN, 44 ml of ethanol and 10 ml of deionized water were put in a flask and vibrated with ultrasonic for 30 min under argon to be dispersed uniformly. Then the flask was heated at 70°C, mechanically stirred at 400 rpm under argon, and a mixture of N-vinyl pyrrolidone (6.4 ml, 0.06 mol), ethanol (7 ml), and deionized water (7 ml) was added dropwise into the flask within 1 h. The graft polymerization was performed at 70°C for 6 h. Then the resultant product was collected by magnetic separation, washed with ethanol for several times, and finally dried at 40°C in a vacuum oven.

2.5. Characterization techniques

Nano- Fe_3O_4 , nano- Fe_3O_4 modified with silan A and also PVP-grafted Fe_3O_4 nanoparticles were tested by Fourier transform infrared (FT-IR) spectroscopy. The measurements were performed on a TENSOR 27 spectrometer (Bruker, Germany) with a solid potassium bromide method, with 2 cm^{-1} resolution and 10 scanning times.

The nanoparticles were observed with transmission electron microscope (TEM) (Jeol TEM-2100, Japan) operated at 200 kV. Investigating TEM, the

nanoparticles were deposited on a copper-grid-supported perforated transparent carbon coil. The crystal structure of prepared nanoparticles was studied by an X-ray diffractometer (Siemens D5000, Germany) using $\text{CuK}\alpha$ radiation ($\lambda = 1.5418 \text{ \AA}$). Particle size distribution was determined by particle size analyzer (Photal ELS Z, Otsuka Electronics, Japan).

Thermogravimetric analysis (TGA) experiments were performed by TGA 951 (DuPont, USA). Dried samples (1–5 mg) were placed in the TGA furnace and the measurements were carried out under nitrogen with a heating rate of 15°C/min from 30 to 650°C. The magnetic properties of Fe_3O_4 nanoparticles were measured at room temperature with vibrating sample magnetometer (VSM) (LakeShore 7307, USA).

MRI experiments were performed at 25°C in a clinical magnetic resonance (MR) scanner (GE Signa EXCITE 1.5T, USA). To demonstrate the T_1 and T_2 effects in an aqueous solution, PVP-grafted magnetic nanoparticles were suspended in tubes of water (10 ml) with iron concentration at 0, 0.025, 0.050, 0.075, 0.100, 0.200, 0.400, and 0.600 mmol/l Fe, respectively. The tubes were placed into the MR scanner and a number of spin-echo sequences were run for determining both T_2 and T_1 relaxation times. The IDL software (version 5.5) was used for data acquisition. To estimate the T_2 relaxation time for each sample, coronal images ($TH = 10 \text{ mm}$) were acquired at various echo times (TE) from 10 to 140 ms with a repetition time (TR) of 1600 ms. Similarly, the T_1 relaxation time for each sample was measured by varying TR between 100 and 6400 ms while keeping TE constant at 18 ms. After acquiring the images, the magnitudes of image intensities were measured within manually-drawn regions of interest (ROIs) for each sample. Relaxation rates R_1 ($1/T_1$) and R_2 ($1/T_2$) were calculated by mono-exponential curve fitting of the signal intensity vs. time (TE or TR). The Equations (1) and (2) were used for curve fitting of relaxation rate R_1 and R_2 , respectively [33]:

For relaxation rate R_1 :

$$I = A \cdot [1 - \exp(-R_1 \cdot TR)] \quad (1)$$

For relaxation rate R_2 :

$$I = A + C \cdot [\exp(-R_2 \cdot TE)] \quad (2)$$

where I is the signal intensity. Plotting R_1 (or R_2) vs. iron concentration gives T_1 relaxivity (r_1) or T_2 relaxivity (r_2) as the slope, respectively.

3. Results and discussion

3.1. Preparation of PVP-grafted Fe_3O_4 nanoparticles

The process for synthesis of PVP-grafted Fe_3O_4 nanoparticles is shown in Figure 1. The Fe_3O_4 nanoparticles were synthesized by a chemical coprecipitation of Fe^{2+} and Fe^{3+} ions under alkaline condition. The concentration ratio of $\text{Fe}^{2+}/\text{Fe}^{3+}$ was 1:2, and the experiment was carried out under argon gas to prevent Fe^{2+} oxidation to Fe^{3+} . The Fe_3O_4 nanoparticles prepared by the co-precipitation method have a number of hydroxyl groups on the surface. Silan A-modified MNPs were achieved by the silanization reaction between silan A and the hydroxyl groups on the surface of magnetite (Figure 1).

Surface-grafted polymerization of N-vinyl pyrrolidone involves two reactions, which take place simultaneously. On the surface of silan A-modified Fe_3O_4 nanoparticles, the graft polymerization occurs, while the random polymerization takes place in the solution. In order to decrease the random polymerization, the following strategies were adopted. On the one hand, AIBN was dissolved in the modified nanoparticles suspended solution and the solution was placed overnight to let nanoparticles absorb AIBN on the surface the most. On the other side, the monomer was added dropwise in the reaction mixture. Following the application of the procedure explained, as the mixture is heated the vinyl groups on the surface of nanoparticles are activated by initiator and when the monomer is

added slowly to the mixture, surface-initiated radical polymerization occurs. The ungrafted oligomers would be separated by magnetic decantation after reaction.

3.2. FT-IR analysis

To evaluate the graft polymerization, the homopolymers and unreacted monomers were extracted from final product within ethanol to be separated from the grafted nanoparticles. Figure 2 shows the FT-IR spectra of pure Fe_3O_4 , silan A-treated Fe_3O_4 and PVP-grafted Fe_3O_4 nanoparticles, respectively. From the IR spectra presented in this figure, the absorption peak at 580 cm^{-1} belongs to the stretching vibration mode of Fe–O bonds in Fe_3O_4 . Comparing with the IR spectrum of pure Fe_3O_4 (Figure 2a), the IR spectrum of Silan A-modified Fe_3O_4 (Figure 2b) has absorption peaks presented at 1700 and 1648 cm^{-1} being relevant to the stretching vibration of conjugated esteric C=O and stretching vibration of C=C bonds, respectively. Absorption bonds of stretching vibrations of esteric C–O bond are appeared at 1172 and 1017 cm^{-1} . Absorbent peaks at 2926 and 1460 cm^{-1} belong to asymmetric stretching vibration and scissoring bending vibration of CH_2 group, respectively. All these peaks revealed the existence of silan A and indicated that the reactive groups had been introduced onto the surface of magnetite. In Figure 2c, the absorbent peak at 1660 cm^{-1} belongs to C=O group of N-vinyl pyrrolidone. Asymmetric stretching and scissoring bending vibrations of CH_2 group of N-vinyl pyrrolidone are appeared at 1957 and 1465 cm^{-1} , respectively. The absorbent peak centered at 1289 cm^{-1} is due to C–N stretching vibration of N-vinyl pyrrolidone. Also the peak at 2957 cm^{-1} is

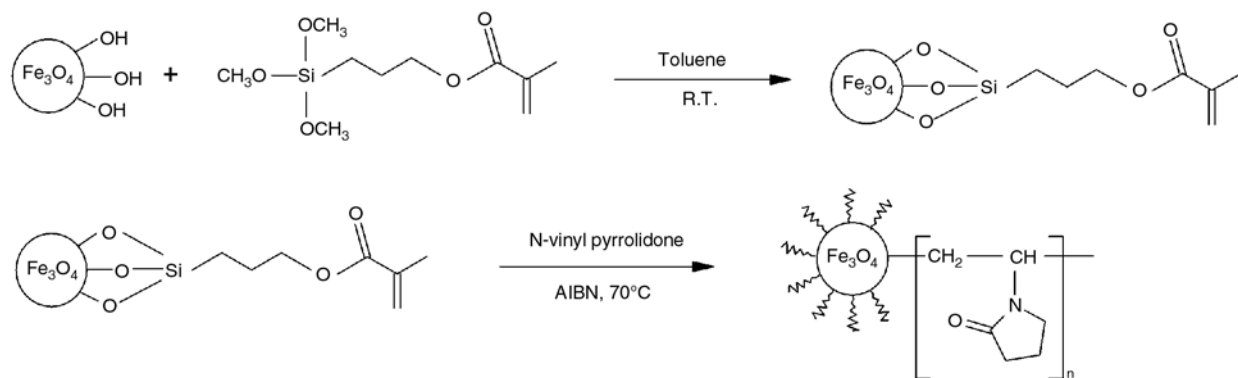


Figure 1. Surface modification and graft polymerization of magnetic nanoparticles

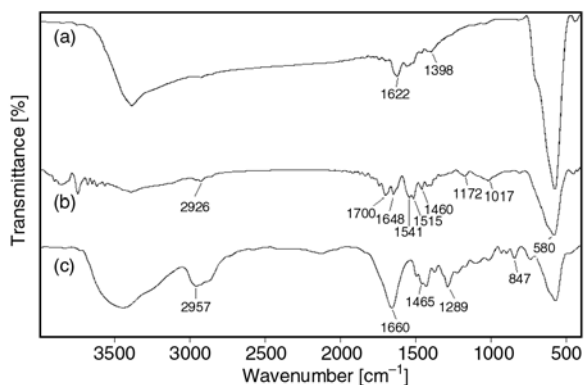


Figure 2. FT-IR spectra of (a) pure Fe₃O₄ nanoparticles; (b) Fe₃O₄ nanoparticles modified with Silan A; (c) PVP-grafted Fe₃O₄ nanoparticles

due to the asymmetric stretching vibration of CH₃ group of azobisisobutyronitrile (AIBN) that is used as initiator. Overall, these FT-IR spectra indicated that N-vinyl pyrrolidone polymer chains were successfully grafted onto the Fe₃O₄ nanoparticles surface.

3.3. X-ray diffraction (XRD)

The XRD diffraction patterns of pure magnetite, silan A treated magnetite and PVP-grafted magnetite nanoparticles are shown in Figure 3a–3c, respectively. It is apparent that the diffraction pattern of our Fe₃O₄ nanoparticles is close to the standard pattern of crystalline magnetite (Figure 3a). The characteristic diffraction peaks marked, respectively, by their indices (220), (311), (400), (422), and (511) could be well indexed to the inverse cubic spinel structure of Fe₃O₄. The average crystallite size *D* was calculated using the Debye-Scherrer formula $D = K\lambda/\beta\cos\theta$, where *K* is

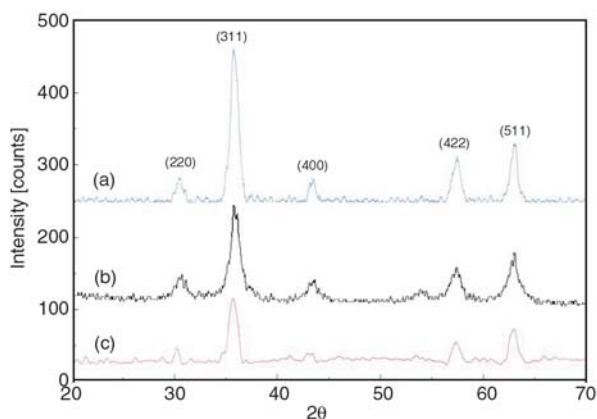


Figure 3. XRD patterns of (a) pure Fe₃O₄ nanoparticles; (b) silan A-modified Fe₃O₄ nanoparticles; (c) PVP-grafted Fe₃O₄ nanoparticles

Table 1. The intensity of magnetite diffraction peaks before and after coating

Diffraction peak	Intensity (counts)		
	Fe ₃ O ₄	Silan A-modified Fe ₃ O ₄	PVP-grafted Fe ₃ O ₄
220	33.32	28.32	25.18
311	212.43	131.39	87.73
400	31.47	26.75	11.02
422	63.73	46.42	26.35
511	81.04	68.06	44.45

Scherrer constant, λ is the X-ray wavelength, β is the peak width of half-maximum, and θ is the Bragg diffraction angle. The crystallite size obtained from this equation was found to be about 19 nm, which is basically in accordance with the transmission electron microscopy. These characteristic peaks can also be found in Figure 3b and 3c, which illustrated that the characteristic peaks did not change but only the peak intensity and width after coated with silan A and PVP, showing that the crystalline structure of the modified nanoparticles was not varied. The intensity of peaks for each sample is given in Table 1.

3.4. Transmission electron microscopy (TEM)

The TEM micrographs of pure Fe₃O₄ nanoparticles (Figure 4a) and Fe₃O₄ nanoparticles grafted by poly(N-vinyl pyrrolidone) (Figure 4b) are shown. Particles with an average diameter of 14 nm were observed. This result is in good accordance with the estimation from X-ray diffraction results. The electron diffraction pattern (Figure 4c) consisting of rings indicates the good crystal structure of the nanoparticles. It can be seen that the particles have a strong tendency to aggregate as a result of the interaction of the polymer grafted on the nanoparticles. This is a further confirmation of the encapsulation of Fe₃O₄ magnetic core polymerized with PVP.

The surface-grafted magnetic nanoparticles could be easily dispersed in water to form a uniform suspension and be stably preserved for several months, suggesting that the tendency for the aggregation of particles is considerably weakened, whereas the suspension made from the bare magnetic nanoparticles is completely precipitated from the solvent in only a few minutes without stirring. Figure 5 shows the size distribution plot for PVP-grafted nanoparticles, as it can be seen the size of nanoparticles has

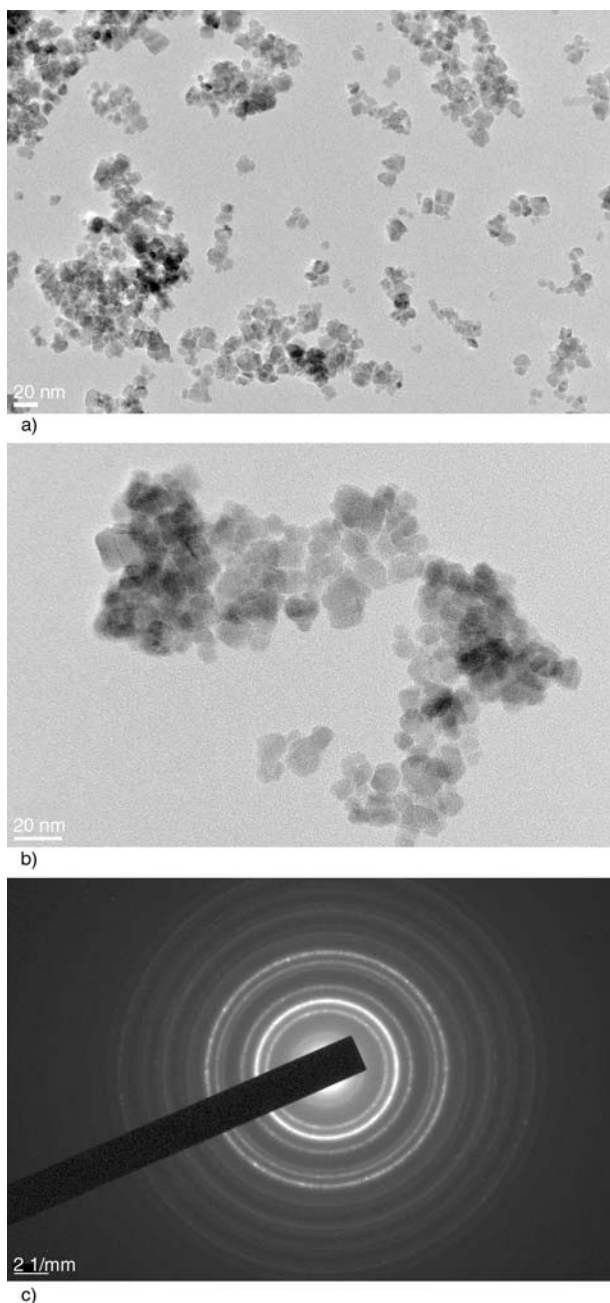


Figure 4. TEM images of (a) pure Fe₃O₄ nanoparticles; (b) PVP-grafted Fe₃O₄ nanoparticles; (c) Electron diffraction pattern of pure Fe₃O₄ nanoparticles

increased because of organic coating and also their aggregation, this is in good agreement with TEM image.

3.5. Thermogravimetric analysis

The magnetite contents of Silan A treated magnetite and PVP-grafted magnetite were measured through the TGA under nitrogen atmosphere condition at the heating rate of 15°C/min. Figure 6 illus-

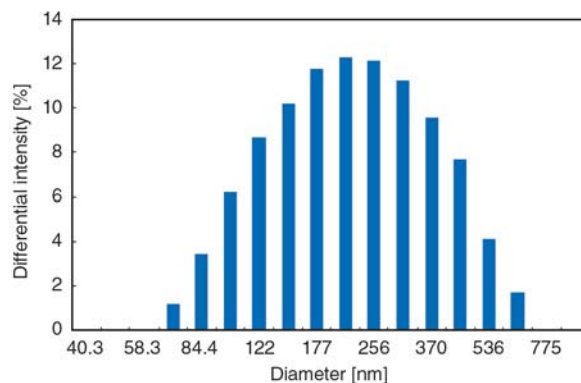


Figure 5. Size distribution plot of PVP-grafted Fe₃O₄ nanoparticles

trates the TGA curves, depicting the variations of residual masses of the samples with temperature. The organic materials and magnetite of the samples were completely burned to generate gas products and converted into Fe₂O₃ at elevated temperatures, respectively. The magnetite amounts of samples can be estimated from the residual mass percentages. The absolute weight loss of the uncoated Fe₃O₄ is 3.2% (Figure 6a) for the whole temperature range because of the removal of adsorbed physical and chemical water. Figure 6b shows that the weight loss increased above 200°C, attributed to the loss of silan A layer coated on the MNPs. It is estimated that the weight loss of silan A coated on the Fe₃O₄ nanoparticles is about 3.8%. As shown in Figure 6c, for PVP-grafted MNPs the first weight loss stage (below 140°C) can be ascribed to the evaporation of water molecules in the polymer matrix, while the other stage beginning at about 200°C was due to the decomposition of PVP. Thermogravimetric chart of PVP-grafted Fe₃O₄ nanopar-

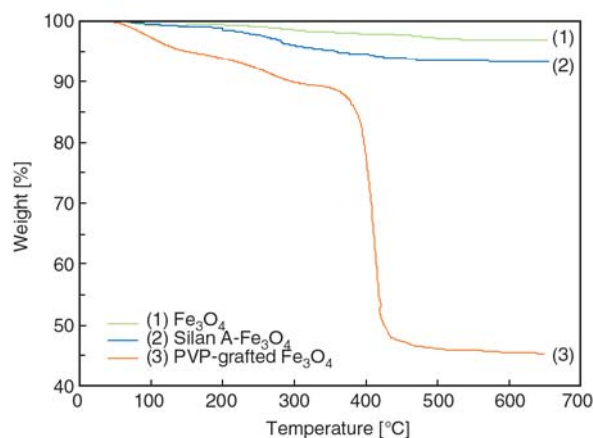


Figure 6. TGA curves of (a) pure Fe₃O₄ nanoparticles; (b) silan A-treated Fe₃O₄ nanoparticles; (c) PVP-grafted Fe₃O₄ nanoparticles

ticles pointed that magnetite content is about 45.3%.

3.6. Analysis of magnetic properties

Figure 7 shows the magnetization curves of pure, silan A-modified, and PVP-grafted Fe₃O₄ nanoparticles respectively, determined by VSM at room temperature. The saturation magnetization (M_s) is found to be 51.6 and 33.5 emu/g for silan A-modified Fe₃O₄ and PVP-grafted Fe₃O₄, respectively, less than the pure Fe₃O₄ nanoparticles (62.1 emu/g). This difference suggests that Silan A and PVP are grafted on the surface of Fe₃O₄ nanoparticles. As M_s of 7–22 emu/g is reported adoptable for bioapplications [34, 35], the level of M_s achieved for PVP-grafted Fe₃O₄ nanoparticles (33.5 emu/g) is deemed sufficient for such applications. In addition, there is no hysteresis in the magnetization curve with both remanence and coercivity being zero, indicating that these magnetic nanoparticles are superparamagnetic.

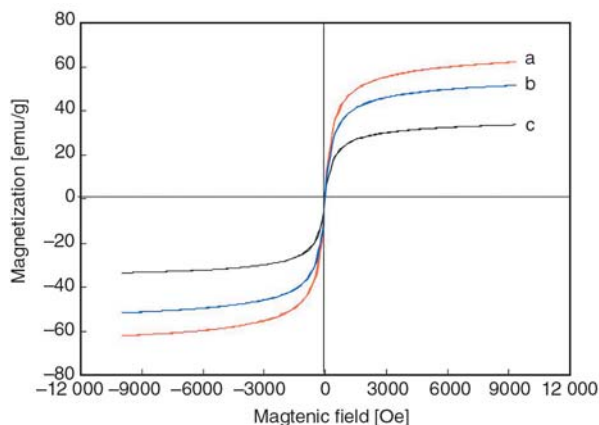


Figure 7. Magnetization curves of (a) pure Fe₃O₄ nanoparticles; (b) Fe₃O₄ nanoparticles treated by Silan A; (c) PVP-grafted Fe₃O₄ nanoparticles

3.7. MRI and relaxivities

Since superparamagnetic Fe₃O₄ nanoparticles are good T_2 -type (negative) contrast agents in MRI, and PVP is a biocompatible macromolecule, the effect of PVP-grafted MNPs was investigated in terms of MR signal-enhancing property. To investigate such a property a phantom test was carried out. Figure 8 shows T_2 -weighted MR images of various concentrations of PVP-grafted Fe₃O₄ nanoparticles in water (spin-echo technique with $TR = 1600$ and $TE = 140$ ms). It can be seen that the MR signal

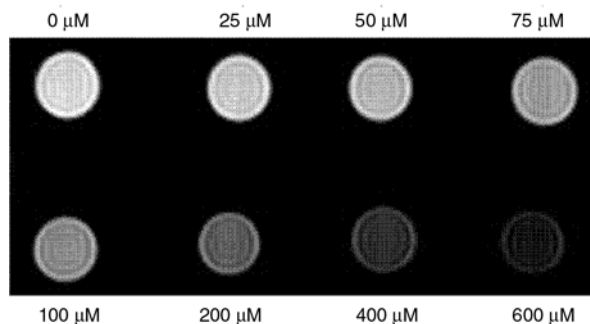


Figure 8. T_2 -weighted MRI images (1.5T, spin-echo sequence: repetition time $TR = 1600$ ms, echo time $TE = 140$ ms) of the PVP-grafted Fe₃O₄ nanoparticles at various iron concentration at 25°C

intensity (related to the T_2 relaxation time in T_2 -weighted images) for the samples of different concentrations is not identical. With increasing nanoparticles concentration in water, the MR signal is enhanced significantly (negative in brightness in T_2 -weighted image). The T_2 relaxation process occurs because of the exchange of energy between protons in water molecules. In the presence of an externally applied magnetic field, superparamagnetic iron oxide nanoparticles create inhomogeneity in the magnetic field affecting the microenvironment that results in dephasing of the magnetic moments of protons and hence T_2 shortening. The results indicate that the nanoparticles can generate high magnetic field gradients near the surface of the PVP-grafted Fe₃O₄ nanoparticles.

Figure 9a and 9b show the relaxation rates R_1 ($R_1 = 1/T_1$) and R_2 ($R_2 = 1/T_2$) as a function of the iron molar concentration, [Fe], for the PVP-grafted MNPs. In Figure 9a and 9b, the relaxation rates R_1 and R_2 were found to vary linearly with the iron concentration, according to the Equations (3) and (4), respectively [36]:

$$\frac{1}{T_1} = \frac{1}{T_1([\text{Fe}] = 0)} + r_1[\text{Fe}] \quad (3)$$

$$\frac{1}{T_2} = \frac{1}{T_2([\text{Fe}] = 0)} + r_2[\text{Fe}] \quad (4)$$

where r_1 and r_2 are the longitudinal and transversal relaxivities, respectively. The intercepts $1/T_1$ ($[\text{Fe}] = 0$) and $1/T_2$ ($[\text{Fe}] = 0$) are the proton inverse relaxation times in pure water. The r_1 value per millimole Fe of the PVP-grafted MNPs is $2.6 \text{ (mmol/l)}^{-1} \cdot \text{s}^{-1}$, while the r_2 value is $72.1 \text{ (mmol/l)}^{-1} \cdot \text{s}^{-1}$. It is well known that the relax-

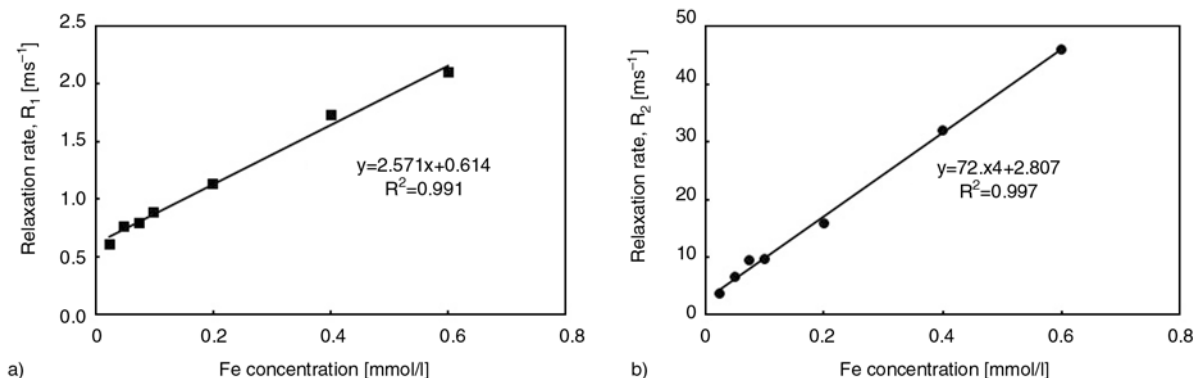


Figure 9. (a) T_1 and (b) T_2 relaxation rates ($1/T_1$ and $1/T_2$ [s⁻¹]) as a function of iron concentration [mmol/l] of PVP-grafted Fe₃O₄ nanoparticles in aqueous solution (1.5T, 25°C)

ivity ratio, r_2/r_1 , is usually an important parameter to estimate the efficiency of T_2 -contrast agents. In our work, the r_2/r_1 is calculated to be 28.1, which is much larger than that of dextran-coated MNPs [37], demonstrating the PVP-grafted MNPs should perform well as T_2 -contrast agents in magnetic resonance imaging.

4. Conclusions

In summary, the present work reports on the preparation of superparamagnetic Fe₃O₄ nanoparticles through co-precipitation method followed by surface modification with poly(N-vinyl pyrrolidone) in two steps. First, magnetite nanoparticles were modified by 3-(trimethoxysilyl) propyl methacrylate (silan A) to introduce reactive groups onto the nanoparticles surface. Second, N-vinyl pyrrolidone was grafted onto the surface of modified-Fe₃O₄ nanoparticles by surface-initiated radical polymerization. The results indicate that the polymer chains had been effectively grafted onto the surface of Fe₃O₄ nanoparticles. The functionalized nanoparticles are superparamagnetic with M_s of 33.5 emu/g and possess good dispersibility and stability in water for a long period of time. MRI of the nanoparticles in water confirmed its contrast enhancement effect in T_2 -weighted sequences. Calculated r_1 and r_2 relaxivities, and also r_2/r_1 ratio indicate that the PVP-grafted nanoparticles may be a good candidate as T_2 contrast agent.

Acknowledgements

The cooperation of Hafez medical imaging center of Tabriz (Dr. Zynat Mayabi, and Mr. Ali Kolahduz) in acquiring the

MRI images is acknowledged. Also, authors gratefully acknowledge the assistance of Mr. Saso Gyergyek and Mr. Slavko Kralj, Joseph Stephan Institute of Slovenia, in the recoding of TEM images and VSM measurements.

References

- [1] Son S. J., Reichel J., He B., Schuchman M., Lee S. B.: Magnetic nanotubes for magnetic-field-assisted bioseparation, biointeraction, and drug delivery. *Journal of American Chemical Society*, **127**, 7316–7317 (2005). DOI: [10.1021/ja0517365](https://doi.org/10.1021/ja0517365)
- [2] Tietze R., Jurgons R., Lyer S., Schreiber E., Wiekhorst F., Eberbeck D., Richter H., Steinhoff U., Trahms L., Alexiou C.: Quantification of drug-loaded magnetic nanoparticles in rabbit liver and tumor after *in vivo* administration. *Journal of Magnetism and Magnetic Materials*, **321**, 1465–1468 (2009). DOI: [10.1016/j.jmmm.2009.02.068](https://doi.org/10.1016/j.jmmm.2009.02.068)
- [3] Liu K. J. W., Zhang Y., Chen D., Yang T., Chen Z. P., Pan S. Y., Gu N.: Facile synthesis of high-magnetization γ -Fe₂O₃/alginate/silica microspheres for isolation of plasma DNA. *Colloids and Surface A: Physicochemical and Engineering Aspects*, **341**, 33–39 (2009). DOI: [10.1016/j.colsurfa.2009.03.033](https://doi.org/10.1016/j.colsurfa.2009.03.033)
- [4] Gupta A. K., Gupta M.: Synthesis and surface engineering of iron oxide nanoparticles for biomedical applications. *Biomaterials*, **26**, 3995–4021 (2005). DOI: [10.1016/j.biomaterials.2004.10.012](https://doi.org/10.1016/j.biomaterials.2004.10.012)
- [5] Zhang L-Y., Gu H-C., Wang X-M.: Magnetite ferrofluid with high specific absorption rate for application in hyperthermia. *Journal of Magnetism and Magnetic Materials*, **311**, 228–233 (2007). DOI: [10.1016/j.jmmm.2006.11.179](https://doi.org/10.1016/j.jmmm.2006.11.179)
- [6] Allard E., Passirani C., Benoit J. P.: Convection-enhanced delivery of nanocarriers for the treatment of brain tumors. *Biomaterials*, **30**, 2302–2318 (2009). DOI: [10.1016/j.biomaterials.2009.01.003](https://doi.org/10.1016/j.biomaterials.2009.01.003)

- [7] Mody V. V., Nounou M. I., Bikram M.: Novel nano-medicine-based MRI contrast agents for gynecological malignancies. *Advanced Drug Delivery Reviews*, **61**, 795–807 (2009).
DOI: [10.1016/j.addr.2009.04.020](https://doi.org/10.1016/j.addr.2009.04.020)
- [8] Liu H., Li J.: Preparation and characterization of poly(PEGMA) modified superparamagnetic nanogels used as potential MRI contrast agents. *Iranian Polymer Journal*, **17**, 721–727 (2008).
- [9] Corti M., Lascialfari A., Micotti E., Castellano A., Donativi M., Quarta A., Cozzoli P. D., Manna L., Pellegrino T., Sangregorio C.: Magnetic properties of novel superparamagnetic MRI contrast agents based on colloidal nanocrystals. *Journal of Magnetism and Magnetic Materials*, **320**, 320–323 (2008).
DOI: [10.1016/j.jmmm.2008.02.064](https://doi.org/10.1016/j.jmmm.2008.02.064)
- [10] Bulte J. W., Hoekstra Y., Kamman R. L., Magin R. L., Webb A. G., Briggs R. W., Go K. G., Hulstaert C. E., Miltenyi S.: Specific MR imaging of human lymphocytes by monoclonal antibody-guided dextran-magnetite particles. *Magnetic Resonance in Medicine*, **25**, 148–157 (1992).
DOI: [10.1002/mrm.1910250115](https://doi.org/10.1002/mrm.1910250115)
- [11] Feng J., Sun G., Pei F., Liu M.: Comparison between GdDTPA and two gadolinium polyoxometalates as potential MRI contrast agents. *Journal of Inorganic Biochemistry*, **92**, 193–199 (2002).
DOI: [10.1016/S0162-0134\(02\)00557-3](https://doi.org/10.1016/S0162-0134(02)00557-3)
- [12] Semelka R. C., Helmberger T. K. G.: Contrast agents for MR imaging of the liver. *Radiology*, **218**, 27–38 (2001).
- [13] Bean C. P., Livingston J. D.: Superparamagnetism. *Journal of Applied Physics*, **30**, 120–129 (1959).
DOI: [10.1063/1.2185850](https://doi.org/10.1063/1.2185850)
- [14] Koenig S. H., Brown R. D.: Relaxometry of magnetic resonance imaging contrast agents. *Magnetic Resonance Annual*, **5**, 263–286 (1987).
- [15] Senéterre E., Taourel P., Bouvier Y., Pradel J., Van Beers B., Daures J. P., Pringot J., Mathieu D., Bruel J. M.: Detection of hepatic metastases: Ferumoxides-enhanced MR imaging versus unenhanced MR imaging and CT during arterial portography. *Radiology*, **200**, 785–792 (1996).
- [16] Kaim A. H., Wischer T., O'Reilly T., Jundt G., Fröhlich J., Schulthess G. K., Allegrini P. R.: MR imaging with ultrasmall superparamagnetic iron oxide particles in experimental soft-tissue infections in rats. *Radiology*, **225**, 808–814 (2002).
DOI: [10.1148/radiol.2253011485](https://doi.org/10.1148/radiol.2253011485)
- [17] Jung C. W., Jacobs P.: Physical and chemical properties of superparamagnetic iron oxide MR contrast agents: Ferumoxides, ferumoxtran, ferumoxsil. *Magnetic Resonance Imaging*, **13**, 661–674 (1995).
DOI: [10.1016/0730-725X\(95\)00024-B](https://doi.org/10.1016/0730-725X(95)00024-B)
- [18] Lacava L. M., Lacava Z. G., Da Silva M. F., Silva O., Chaves S. B., Azevedo R. B., Pelegrini F., Gansau C., Buske N., Sabolovic D., Morais P. C.: Magnetic resonance of a dextran-coated magnetic fluid intravenously administered in mice. *Biophysical Journal*, **80**, 2483–2486 (2001).
DOI: [10.1016/S0006-3495\(01\)76217-0](https://doi.org/10.1016/S0006-3495(01)76217-0)
- [19] Strable E., Bulte J. M., Moskowitz B., Vivekanandan K., Allen M., Douglas T.: Synthesis and characterization of soluble iron oxide-dendrimer composites. *Chemistry of Materials*, **13**, 2201–2209 (2001).
DOI: [10.1021/cm010125i](https://doi.org/10.1021/cm010125i)
- [20] Kohler N., Sun C., Fichtenholtz A., Gunn J., Fang C., Zhang M. Q.: Methotrexate-immobilized poly(ethylene glycol) magnetic nanoparticles for MR imaging and drug delivery. *Small*, **2**, 785–792 (2006).
DOI: [10.1002/smll.200600009](https://doi.org/10.1002/smll.200600009)
- [21] Lee H-Y., Lee S-H., Xu C., Xie J., Lee J-H., Wu B., Koh A. L., Wang X., Sinclair R., Wang S. X., Nishimura D. G., Biswal S., Sun S., Cho S. H., Chen X.: Synthesis and characterization of PVP-coated large core iron oxide nanoparticles as an MRI contrast agent. *Nanotechnology*, **19**, 165101/1–165101/6 (2008).
DOI: [10.1088/0957-4484/19/16/165101](https://doi.org/10.1088/0957-4484/19/16/165101)
- [22] Liu H-L., Ko S. P., Wu J-H., Jung M-H., Min J. H., Lee J. H., An B. H., Kim Y. K.: One-pot polyol synthesis of monosize PVP-coated sub-5 nm Fe₃O₄ nanoparticles for biomedical applications. *Journal of Magnetism and Magnetic Materials*, **310**, 815–817 (2007).
DOI: [10.1016/j.jmmm.2006.10.776](https://doi.org/10.1016/j.jmmm.2006.10.776)
- [23] Lee H. Y., Lim N. H., Seo J. A., Yuk S. H., Kwak B. K., Khang G., Lee H. B., Cho S. H.: Preparation and magnetic resonance imaging effect of polyvinylpyrrolidone-coated iron oxide nanoparticles. *Journal of Biomedical Materials Research B: Applied Biomaterials*, **79**, 142–150 (2006).
DOI: [10.1002/jbm.b.30524](https://doi.org/10.1002/jbm.b.30524)
- [24] Garrec D. L., Gori S., Luo L., Lessard D., Smith D. C., Yessine M. A., Ranger M., Leroux J. C.: Poly(*N*-vinylpyrrolidone)-block-poly(D,L-lactide) as a new polymeric solubilizer for hydrophobic anticancer drugs: *In vitro* and in vivo evaluation. *Journal of Controlled Release*, **99**, 83–101 (2004).
DOI: [10.1016/j.jconrel.2004.06.018](https://doi.org/10.1016/j.jconrel.2004.06.018)
- [25] Lee H., Lee E., Kim D. K., Jang N. K., Jeong Y. Y., Jon S.: Antibiofouling polymer-coated superparamagnetic iron oxide nanoparticles as potential magnetic resonance contrast agents for in vivo cancer imaging. *Journal of American Chemical Society*, **128**, 7383–7389 (2006).
DOI: [10.1021/ja061529k](https://doi.org/10.1021/ja061529k)

- [26] Kohler N., Fryxell G. E., Zhang M.: A bifunctional poly(ethylene glycol) silane immobilized on metallic oxide-based nanoparticles for conjugation with cell targeting agents. *Journal of American Chemical Society*, **126**, 7206–7211 (2004).
DOI: [10.1021/ja049195r](https://doi.org/10.1021/ja049195r)
- [27] Feng B., Hong R. Y., Wang L. S., Guo L., Li H. Z., Ding J., Zheng Y., Wei D. G.: Synthesis of Fe₃O₄/APTES/PEG diacid functionalized magnetic nanoparticles for MR imaging. *Colloids and Surfaces A: Physicochemical and Engineering Aspects*, **328**, 52–59 (2008).
DOI: [10.1016/j.colsurfa.2008.06.024](https://doi.org/10.1016/j.colsurfa.2008.06.024)
- [28] Barrera C., Herrera A. P., Rinaldi C.: Colloidal dispersions of monodisperse magnetite nanoparticles modified with poly(ethylene glycol). *Journal of Colloid and Interface Science*, **329**, 107–113 (2009).
DOI: [10.1016/j.jcis.2008.09.071](https://doi.org/10.1016/j.jcis.2008.09.071)
- [29] Cao H., He J., Deng L., Gao X.: Fabrication of cyclodextrin-functionalized superparamagnetic Fe₃O₄/amino-silane core-shell nanoparticles via layer-by-layer method. *Applied Surface Science*, **225**, 7974–7980 (2009).
DOI: [10.1016/j.apsusc.2009.04.199](https://doi.org/10.1016/j.apsusc.2009.04.199)
- [30] Fan Q-L., Neoh K-G., Kang E-T., Shuter B., Wang S-C.: Solvent-free atom transfer radical polymerization for the preparation of poly(poly(ethyleneglycol) monomethacrylate)-grafted Fe₃O₄ nanoparticles: Synthesis, characterization and cellular uptake. *Biomaterials*, **28**, 5426–5436 (2007).
DOI: [10.1016/j.biomaterials.2007.08.039](https://doi.org/10.1016/j.biomaterials.2007.08.039)
- [31] Yong Y., Bai Y., Li Y., Lin L., Cui Y., Xia C.: Preparation and application of polymer-grafted magnetic nanoparticles for lipase immobilization. *Journal of Magnetism and Magnetic Materials*, **320**, 2350–2355 (2008).
DOI: [10.1016/j.jmmm.2008.04.158](https://doi.org/10.1016/j.jmmm.2008.04.158)
- [32] Massart R., Cabuil V.: Effect of some parameters on the formation of colloidal magnetite in alkaline medium: Yield and particle size control. *Journal of Chemical Physics*, **84**, 967–973 (1987).
- [33] Jain T. K., Richey J., Strand M., Leslie-Plecky D. L., Flask C. A., Labhasetwar V.: Magnetic nanoparticles with dual functional properties: Drug delivery and magnetic resonance imaging. *Biomaterials*, **29**, 4012–4021 (2008).
DOI: [10.1016/j.biomaterials.2008.07.004](https://doi.org/10.1016/j.biomaterials.2008.07.004)
- [34] Brusentsov N. A., Gogosov V. V., Brusentsova T. N., Sergeev A. V., Jurchenko N. Y., Kuznetsov A. A., Kuznetsov O. A., Shumakov L. I.: Evaluation of ferromagnetic fluids and suspensions for the site-specific radiofrequency-induced hyperthermia of MX11 sarcoma cells in vitro. *Journal of Magnetism and Magnetic Materials*, **225**, 113–117 (2001).
DOI: [10.1016/S0304-8853\(00\)01238-5](https://doi.org/10.1016/S0304-8853(00)01238-5)
- [35] Xu C. J., Xu K. M., Gu H. W., Zhong X. F., Guo Z. H., Zheng R., Zhang X., Xu B.: Nitrilotriacetic acid-modified magnetic nanoparticles as a general agent to bind histidine-tagged proteins. *Journal of American Chemical Society*, **126**, 3392–3393 (2004).
DOI: [10.1021/ja031776d](https://doi.org/10.1021/ja031776d)
- [36] Gillis P., Koenig S. H.: Transverse relaxation of solvent protons induced by magnetized spheres: Application to ferritin, erythrocytes, and magnetite. *Magnetic Resonance in Medicine*, **5**, 323–345 (1987).
DOI: [10.1002/mrm.1910050404](https://doi.org/10.1002/mrm.1910050404)
- [37] Wang Y-X. J., Hussain S. M., Krestin G. P.: Superparamagnetic iron oxide contrast agents: Physicochemical characteristics and applications in MR imaging. *European Radiology*, **11**, 2319–2331 (2001).
DOI: [10.1007/s003300100908](https://doi.org/10.1007/s003300100908)